Adaptive AFM scan speed control for high aspect ratio fast structure tracking

Ahmad Ahmad, Andreas Schuh, and Ivo W. Rangelow
Department of Microelectronic and Nanoelectronic Systems, Faculty of Electrical Engineering and Information Technology Ilmenau University of Technology, Gustav-Kirchhoffstr. 1, 98684 Ilmenau, Germany

(Received 15 April 2014; accepted 21 September 2014; published online 8 October 2014)

Improved imaging rates in Atomic Force Microscopes (AFM) are of high interest for disciplines such as life sciences and failure analysis of semiconductor wafers, where the sample topology shows high aspect ratios. Also, fast imaging is necessary to cover a large surface under investigation in reasonable times. Since AFMs are composed of mechanical components, they are associated with comparably low resonance frequencies that undermine the effort to increase the acquisition rates. In particular, high and steep structures are difficult to follow, which causes the cantilever to temporarily loose contact to or crash into the sample. Here, we report on a novel approach that does not affect the scanner dynamics, but adapts the lateral scanning speed of the scanner. The controller monitors the control error signal and, only when necessary, decreases the scan speed to allow the z-piezo more time to react to changes in the sample's topography. In this case, the overall imaging rate can be significantly increased, because a general scan speed trade-off decision is not needed and smooth areas are scanned fast. In contrast to methods trying to increase the z-piezo bandwidth, our method is a comparably simple approach that can be easily adapted to standard systems. © *2014 AIP Publishing LLC*. [http://dx.doi.org/10.1063/1.4897141]

I. INTRODUCTION

Atomic Force Microscopes (AFM) are mechanical constructions equipped with electro-mechanical transducers and cantilever beams.[1] Either the sample or the cantilever is moved to image a sample's topography or other surface properties. As such, the scan speeds are mainly limited due to the mechanical dynamics of the scanner and the cantilever. However, high speed scanning is important for disciplines where fast sample dynamics need to be resolved or large areas have to be covered. For example, the former is the case in life sciences, where biological samples in fluid need to be observed in fractions of a second to capture its dynamics.

The scanner has three degrees of freedom in order to move the sample (or cantilever) in all spatial directions. Different requirements are set for each axis. The in-plane axes x and y generally follow a triangular actuation signal pattern and high resonances of the scanner structures are needed, so that the very same are not excited at higher scan speeds. Many different techniques on suppressing resonances in the lateral movement have been proposed before.[2–6] The vertical out of-plane z axis follows the topography of the sample. In this case, the shape of sample directly influences the quality of the scan and its maximum allowable scan speed. Different approaches have been developed to increase the tracking speed of the z axis by different means, such as the dual actuator principle,[7,8] using piezo-stacks instead of a tube scanner,[9,10] counter z balancing,[11,12] or a H_∞ controller instead of a PID controller.[13]

Also, structures with high variations in their heights (high aspect ratios) are harder to follow than small ones. This is mainly due to the saturation problem of the error signal, because, e.g., a cantilever scanning above a steep downward step can temporarily become free from the sample. The amplitude of the cantilever will approach the free air amplitude, where damping through the surface is absent. At this point, the amplitude stops increasing and the error will be constant, independent of the distance of the cantilever to the surface. Equipped with a regular PID controller, the cantilever takes a prolonged time to get back to the sample surface. A similar problem appears, when the cantilever is hitting an upward step and the amplitude becomes completely suppressed by the surface features. Dynamic PID control has been developed to tackle this problem, where the error signal is artificially increased beyond a set threshold.[14] In case that the cantilever loses track of the surface and approaches its free amplitude, the error signal is multiplied by a constant. The unmodified PID controller parameters now act on a higher error signal, resulting in a higher control action of the z-piezo. This is equivalent to temporarily increasing the gains of the PID controller. Hence, the cantilever is brought back to contact faster. But the increased feedback bandwidths are also vulnerable to instabilities caused by the controller. Thus, this technique has an upper limit in increasing the speed. A different approach is the adaptive Q control.[15] Here, a threshold in the error signal is used to switch between different cantilever Q factors, causing a modified imaging bandwidth. In order to not lose track of the surface at deep steps, the Q factor is increased. This also increases the amplitude, in turn maintaining the contact to the surface. The disadvantage lies in the increased Q factor that also inherits a decreased imaging bandwidth. In addition, very high Q factors can lead to instabilities.

In this paper, we introduce an adaptive approach that modifies the scan speed of the lateral scanner axes to increase the imaging quality of the z axis. It is based on the error signal created by the topography feedback controller. The

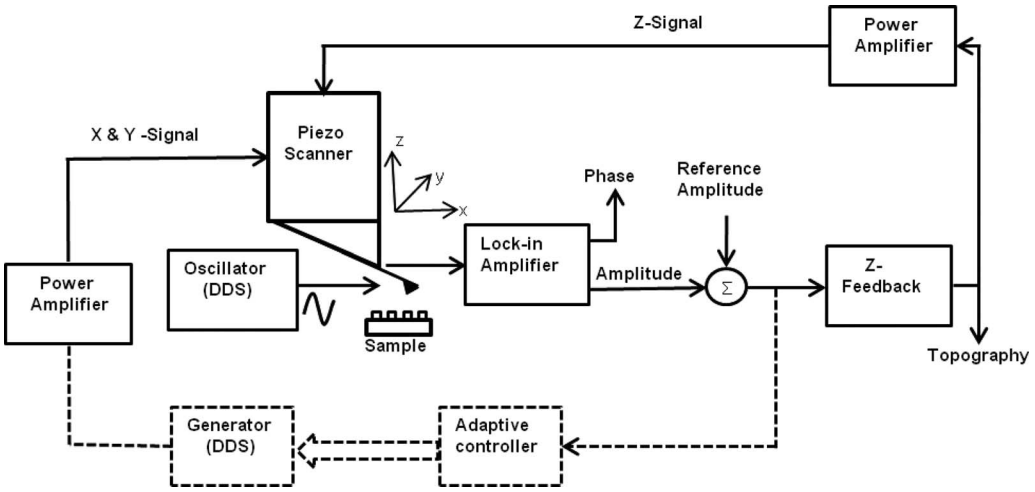

FIG. 1. AFM setup extended by the adaptive controller, which is indicated by the gray and dashed lines.

error is defined as the difference between the set-point and the cantilever's amplitude of vibration. High error signals indicate suboptimal tracking, meaning that the cantilever is not following the topography well at its given set-point. As such, when the error signal increases beyond a threshold, the scanning velocities in the x and y directions are reduced. Hence, instead of increasing the z feedback gains, we allow the z axis an extended time to adapt to topographical changes. The adaptive controller is connected to an AFM setup, as indicated by the gray dashed lines and boxes in Figure 1.

The paper is organized as follows. Section II describes the modified AFM setup, where the technique is implemented and tested. Section III introduces the problem in detail, which forms the basis for the controller analysis, and design is given in Sec. IV. Section V covers the measurement results, followed by a conclusion in Sec. VI.

II. EXPERIMENTAL SETUP

In the following, the components of the AFM system are introduced that have been to most parts developed and fabricated in our group. This includes the 3D scanning stage, cantilevers, feedback controller, high voltage amplifiers, and PC control software. The feedback controller is a FPGA based system that, in its core function, generates the signals for the lateral movement of the scanner, applies the sinusoidal actuation signal to the cantilever's integrated actuator, obtains the cantilever's AC amplitude and phase via a digital Lock-in amplifier, and generates a control signal for the z-piezo. The setup in Figure 1 shows the overall AFM configuration in a block diagram.

Unlike regular commercial available cantilevers, we have fabricated and used cantilevers with integrated actuation and sensing.[16,17] The actuation is achieved by stacking materials of different thermal expansion coefficients together. One of them is electrically conductive and shaped in a way to efficiently convert the electrical current into heat. The produced heat causes both materials to expand, one of them more than the other. As the two materials are connected, the cantilever bends into the vertical direction of the material with the lower coefficient. By applying an AC current, the cantilever thus can be actuated at its resonance. The sensors are based on the piezo-resistive effect in silicon.[18,19] Upon bending, the implanted sensors change their resistivity proportional to the cantilever's tip displacement. The sensors are located close to the base of the cantilever, where the highest bending strain is induced.

The utilized top-scanner moves the cantilever instead of a sample. The cantilever and its holder are often lower in mass than the moving part of the scanner and sample, which is beneficial for increasing the scan rate. The constant top-scanner load is also of benefit for certain resonance compensating algorithms. On the other hand, a slightly more difficult setup is imposed, since the wires connected to the cantilevers are now moved as well. The high voltage/current amplifier generates the signals for the piezo-actuators of the scanner. It needs to be able to drive the high capacities of the piezos at high voltage, requiring specialized components.

III. ERROR SATURATION PROBLEM FORMULATION

As indicated before, a problem appears in the intermittent AFM mode by scanning surfaces with relatively high topographic aspect ratios, resulting in error saturations. This is in particular pronounced at high imaging rates. Figure 2 shows such an error signal, where a sharp downward and upward step are scanned. The saturation causes the feedback controller to operate in an open loop condition that increases the time to settle back the cantilever oscillations to its setpoint. It leads to non-sharp, sloping edges at both steps in the topographic image.

The two different cases of scanning downward and upward steps are introduced in the following.

Case I: At a sharp downward step the cantilever becomes far away from the sample surface and the oscillation amplitude A approaches the free air amplitude A_f. The error signal, the difference of A and setpoint A_{set}, reaches a constant value E_{down}:

$$E_{down} = A - A_{set} = A_f - A_{set}. \quad (1)$$

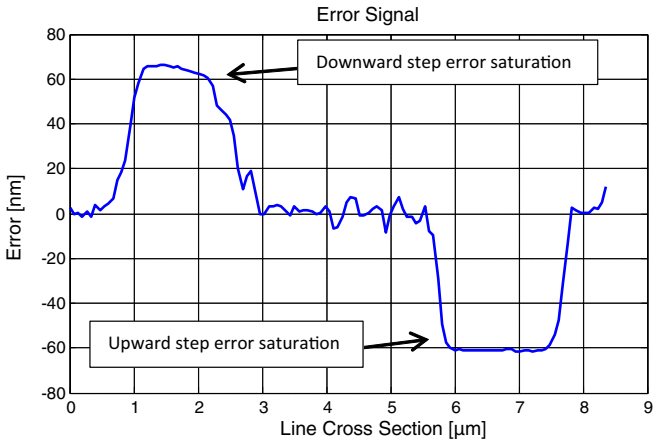

FIG. 2. Error signal showing the problematic error saturation at ±60 nm causing prolonged control action.

Assuming $A_f = 120\ nm$ and an A_{set} of 50% results in

$$E_{down} = A_f - \frac{1}{2}A_f = 60\,\text{nm}. \tag{2}$$

The error remains at E_{down}, until the cantilever is again close to the surface.

Case II: At a sharp upward step the cantilever clashes into the surface and the oscillation amplitude becomes very small or even completely suppressed. In the latter case the error is limited by its maximum value E_{up}:

$$E_{up} = A - A_{set} = -A_{set}. \tag{3}$$

With a similar setpoint assumption as in Case I, the error saturation results in

$$E_{up} = -\frac{1}{2}A_f = -60\,\text{nm}. \tag{4}$$

The error remains at E_{up} until the z piezo is retracted far enough to allow the cantilever to oscillate again at its tip. The time constants involved are similar to the ones in Case I.

IV. DYNAMIC SCAN SPEED CONTROLLER

In this work, the scan speeds in x and y directions are modified adaptively depending on the topography error signal $E = A - A_{set}$. Consequently, the scanner signal frequencies in x and y directions are reduced, when the error exceeds a set negative or positive value. Such decrease in the scan speed allows the feedback in the vertical z direction to properly respond to the edges of the scanned surface structures.

Following, the scanning rate V in lines/s can be described as

$$V = \begin{cases} k_d V_0 & when \quad E \geq E_{+S} \\ k_u V_0 & when \quad E \leq E_{-S} \\ V_0 & when \quad E_{+S} > E > E_{-S} \end{cases}, \tag{5}$$

where V_0 is the standard line scan rate. k_d and k_u are coefficients that define the reduced scan speed. They must be smaller than one and chosen beforehand. E_{+S} and E_{-S} are the positive and negative error threshold, respectively. The thresholds are chosen to satisfy:

$$\begin{aligned} 0 &< E_{+S} < E_{down}, \\ 0 &> E_{-S} > E_{up}. \end{aligned} \tag{6}$$

The line scan frequency f_x drives the piezo in x direction. It is equivalent to the line scan rate V that directly translates into f_x. For example, a V of 10 lines/s corresponds to a scan frequency of 10 Hz. The scan frequency f_y drives the piezo in y direction and forms an image acquisition rate. Here, half a period can obtain a full image of a given number of lines. Both frequencies are derived as

$$\begin{aligned} f_x &\sim V, \\ f_y &\sim \tfrac{V}{2(R_y - 1)}, \end{aligned} \tag{7}$$

where R_y is the resolution in y direction, which is equivalent to the number of lines in the image.

The signals of frequencies $f_{x,y}$ driving the scanner in the respective lateral directions can be generated by using Direct Digital Synthesis (DDS) generators in the FPGA controller. The input to the DDS generators is phase increment values $d\phi_{x,y}$. They are functions of the generators' accumulator bit-width B, its clock frequency f_{clk}, and $f_{x,y}$:

$$f_{x,y} = \frac{f_{clk} d\phi_{x,y}}{2^B} \Rightarrow d\phi_{x,y} = \frac{2^B f_{x,y}}{f_{clk}}. \tag{8}$$

The final scanner actuation signals are generated by logical arrangements that convert the intermediate outputs of the DDS into the desired triangular or sinusoidal signals. Hence, $d\phi_{x,y}$ is used to modify the scan rate V of Eq. (5). The algorithm was implemented into the AFM FPGA controller. In Sec. V, we will show that the adaptive scan speed controller solves the error saturation problem and allows achieving accurate topography images of a surface at higher scanning speeds.

V. EXPERIMENTAL RESULTS

In this section, imaging results are presented to indicate the effectiveness of the adaptive controller. Figure 3 compares topographic images obtained under three different conditions with a scan speed of 30 lines/s. The free amplitude was chosen to $A_f = 120$ nm and a set point of $A_{set} = 90$ nm. The slow scan direction was in the vertical image direction. Figure 3(a) shows an image scanned without the adaptive modification and regular PID settings, where the sloped edges are clearly visible. In Figure 3(b), the integrator time constant of the PID controller was decreased, causing a faster response to topographical changes. However, oscillations occur as a result of the reduced phase/gain margins. Figure 3(c) is an image obtained with the adaptive scan speed controller and regular PID settings. The feature was clearly resolved with sharp edges. Different cross sections of the topographic images are shown in Figure 3(d). The dashed green, dashed red, and blue curves refer to regular image conditions, decreased integrator time constant, and usage of the adaptive controller, respectively. The cross sections are indicated by white lines in Figures 3(a)–3(c).

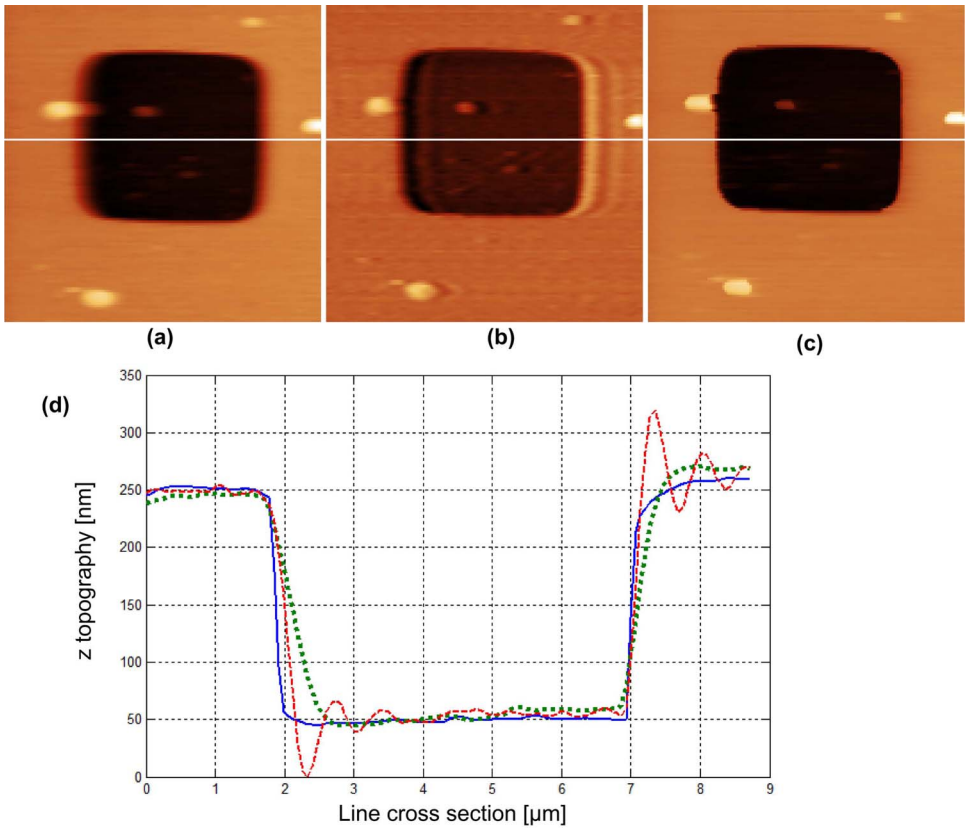

FIG. 3. (a) Topographic image showing sloped steps resulting from the error saturation, (b) vibrations occur as a result of an increased integral gain in an attempt to speed up the imaging, (c) topographic image obtained by using the adaptive scan speed controller. (d) indicates the different cross sections of the images in (a)-(c): the dashed green, dashed red, and blue curves refer to subfigures (a), (b), and (c), respectively, where the locations of the cross sections are indicated by a white line. The scan speed was 30 lines/s in all cases.

The slopes of the steps were considerably improved. Under regular imaging conditions, the slopes were −0.29 and 0.37 for the downward and upward step, respectively (dashed green curve in Figure 3(d)). The increased feedback gain resulted in slopes of −0.6 and 0.85 (dashed red curve). The adaptive controller enhanced the slopes to −1.3 and 1.4 (blue curve). All slopes are dimensionless, since the components to determine it carry similar units. Hence, the overall scan frequencies $f_{x,y}$ could be chosen much higher with the included adaptive controller, such that smooth areas are scanned quickly. Since the decreased scanning frequencies only occur on edges of high aspect ratios, the image acquisition rate is not considerably decreased.

Figure 4 shows additional topographic images and cross sections at different scan rates. Figures 4(a) and 4(b) are images obtained without and with the adaptive controller, respectively. The acquisition rate was at 4 lines/s and the PID settings were not modified. The corresponding cross sections are shown in Figure 4(c), with the dashed green and blue curves corresponding to the imaging conditions in Figures 4(a) and 4(b), respectively. The slopes of the features in Figure 4(c) were improved from −0.5 and 0.4 (dashed green curve) for the downward and upward step to −2.1 and 2.1 (blue curve), respectively. This also approximately represents the maximum achievable slope based on the slow imaging rate.

The imaging conditions in Figures 4(d), 4(g), 4(e), and 4(h) and the cross sections in Figure 4(f) and 4(i) are equivalent to Figures 4(a)–4(c), respectively, but with different acquisition rates of 50 and 100 lines/s as indicated. Here, the slopes of the features in Figure 4(f) were improved from −0.18 and 0.24 (dashed green curve) for the downward and upward step to −0.75 and 1.1 (blue curve), respectively. Similarly, the slopes of the features in Figure 4(i) were improved from −0.06 and 0.18 to −0.44 and 0.95, respectively. For example, by comparing Figure 4(h) obtained at 100 lines/s (adaptive controller) with Figure 4(a) obtained at 4 lines/s (regular imaging) it can be noted that the slopes for the downward steps are similar. It indicates that the imaging rate can be sped up by 25 times without losing step resolution.

In addition, a larger setpoint can be used with an active adaptive scan speed controller. This means that A_{set} can be chosen close to A_f, resulting in a smaller force applied on the surface. This is, in particular, important for imaging soft samples, such as cells used in biological applications. Imaging with a large set point worsens the effect of error saturation in the case of downward steps. Figure 5 shows a comparison between regular AFM imaging and by using the adaptive scan speed controller. In this case, the slopes were improved from −0.05/0.18 to −0.83/1.00.

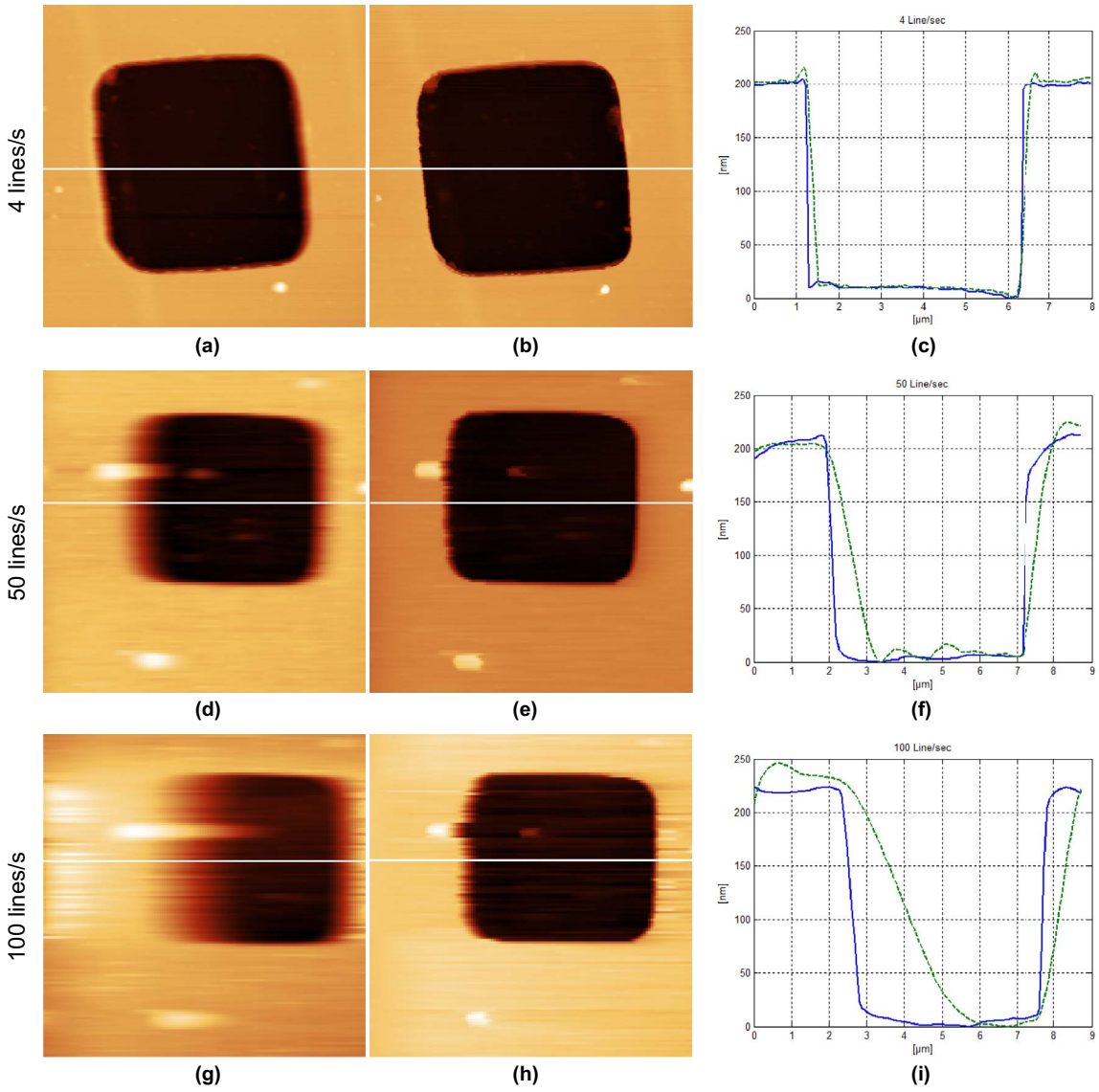

FIG. 4. (a), (d), and (g) are topographic images showing sloped steps resulting from the error saturation at 4 lines/s, 50 lines/s, and 100 lines/s, respectively. (b), (e), and (h) are topographic images obtained by using the adaptive scan speed controller at 4 lines/s, 50 lines/s, and 100 lines/s, respectively. (c), (f), and (i) are different cross sections at 4 lines/s, 50 lines/s, and 100 lines/s, respectively; the dashed green curves refer to the regular imaging and the blue curves by using the adaptive controller.

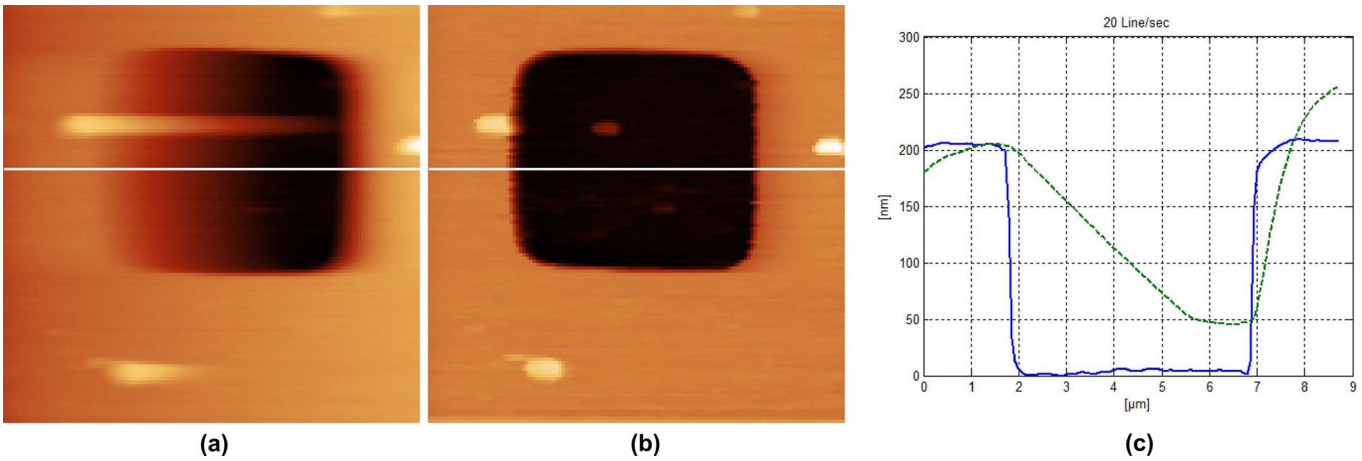

FIG. 5. (a) Soft imaging without and (b) with the adaptive scan speed controller; (c) is a cross section comparing the two cases. The dashed green curve refers to the regular imaging and the blue curve by using the adaptive controller. Images taken at 20 lines/s.

TABLE I. Summary of slopes and ratios indicated throughout the text for better comparison.

Imaging rate (lines/s)	Slope regular imaging	Slope imaging with adaptive controller	Ratio of improvement
4 (downward)	− 0.5	− 2.1	4.2
4 (upward)	0.4	2.1	5.3
30 (downward)	− 0.29	− 1.3	4.5
30 (upward)	0.37	1.4	3.8
50 (downward)	− 0.18	− 0.75	4.2
50 (upward)	0.24	1.1	4.6
100 (downward)	− 0.06	− 0.44	7.3
100 (upward)	0.18	0.95	5.3
20 (downward, LSP)	− 0.05	− 0.83	16.6
20 (upward, LSP)	0.18	1.00	5.6

Table I summarizes the various different slopes and its ratios for better comparison. The large setpoint condition is indicated as LSP.

VI. CONCLUSION

We have demonstrated an alternative approach, namely, an adaptive scan speed controller, to increase the imaging speed despite limitations of the vertical z axis. In particular, steep edges are often only present in a small fraction of the overall image. Thus, most of the topography can be scanned with a fast velocity. Only when the error signal is exceeding a given threshold value, the imaging speed is reduced to allow the z axis to get back to the setpoint. This technique also avoids the saturation of the error that needs prolonged times to recover from. Due to the nature of our technique the step resolution is significantly increased at similar line acquisition rates. Consequently, the imaging speed can be increased by 4-6 times on average for medium setpoints, keeping an image quality (step-resolution) comparable to the absence of the adaptive controller. In case of large setpoints, the improvement was even up to 17 fold. Furthermore, the scan speed does not need to be compromised to a single acquisition rate over the entire image. This takes away some of the need to find a trade-off between accurate tracking (slower at edges) and imaging speed (faster at smooth places).

ACKNOWLEDGMENTS

This work was financially supported in the frame of the Collaborative Research Centre 622 (SFB 622) by the German Research Foundation (DFG).

[1]G. Binnig, C. F. Quate, and Ch. Gerber, Phys. Rev. Lett. **56**, 930 (1986).
[2]D. J. Burns, K. Youcef-Toumi, and G. E. Fantner, Nanotechnology **22**(31), 315701 (2011).
[3]S. Salapaka, A. Sebastian, J. P. Cleveland, and M. V. Salapaka, Rev. Sci. Instrum. **73**(9), 3232 (2002).
[4]G. Schitter and A. Stemmer, Microelectronic. Eng. **67–68**, 938 (2003).
[5]G. Schitter, K. J. Åström, B. DeMartini, G. E. Fantner, K. Turner, P. J. Thurner, and P. K. Hansma, in *Proceedings of the 2006 American Control Conference Minneapolis*, Minnesota, USA (14–16 June 2006).
[6]E. Guliyev, B. E. Volland, Y. Sarov, Tzv. Ivanov, M. Klukowski, E. Manske, and I. W. Rangelow, Meas. Sci. Technol. **23**, 074012 (2012).
[7]K. El Rifai, O. El Rifai, and K. Youcef-Toumi, in *Proceedings of the 2004 American Control Conference*, Boston, MA, 30 June–2 July 2004, pp. 3128–3133.
[8]G. E. Fantner, D. J. Burns, A. M. Belcher, I. W. Rangelow, and K. Youcef-Toumi, J. Dyn. Sys., Meas., Control **131**(6), 061104 (2009) (13 pages).
[9]J. H. Kindt, G. E. Fantner, J. A. Cutroni, and P. K. Hansma, Ultramicroscopy **100**(3–4), 259 (2004).
[10]A. Sebastian and S. M. Salapaka, IEEE Trans. Control Syst. Technol. **13**(6), 868 (2005).
[11]N. Kodera, H. Yamashita, and T. Ando, Rev. Sci. Instrum. **76**(5), 053708 (2005).
[12]I. S. Bozchalooi, K. Youcef-Toumi, D. J. Burns, and G. E. Fantner, Rev. Sci. Instrum. **82**, 113712 (2011).
[13]G. Schitter, F. Allgower, and A. Stemmer, Nanotechnology **15**(1), 108 (2004).
[14]N. Kodera, M. Sakashita, and T. Ando, Rev. Sci. Instrum. **77**, 083704 (2006).
[15]I. Gunev, A. Varol, S. Karaman, and C. Basdogan, Rev. Sci. Instrum. **78**, 043707 (2007).
[16]R. Pedrak, Tzv. Ivanov, T. Gotszalk,P. Hudek, O. Fortagne, and I. W. Rangelow, J. Vac. Sci. Technol. B **21**(6), 3102–3107 (2003).
[17]Tzv. Ivanov, T. Gotszalk, P. Grabiec, E. Tomerov, and I. W. Rangelow, Microelectron. Eng. **67–68**, 550–556 (2003).
[18]Tzv. Ivanov, T. Gotszalk, T. Sulzbach, I. Chakarov, and I. W. Rangelow, Microelectron. Eng. **67–68**, 534–541 (2003).
[19]Tzv. Ivanov, T. Gotszalk, T. Sulzbach, and I. W. Rangelow, Ultramicroscopy **97**(1–4), 377–384 (2003).